



**HAL**  
open science

# Compact Efficient and Frequency Tunable Relativistic Magnetron With Reducing Coaxial Section and Tilted Tuners

Yannick Delvert, Antoine Chauloux, Jean-Christophe Diot, Thierry Chanconie, Nicolas Ribière-Tharaud, Philippe Lévêque

► **To cite this version:**

Yannick Delvert, Antoine Chauloux, Jean-Christophe Diot, Thierry Chanconie, Nicolas Ribière-Tharaud, et al.. Compact Efficient and Frequency Tunable Relativistic Magnetron With Reducing Coaxial Section and Tilted Tuners. IEEE Transactions on Electron Devices, 2023, 70 (8), pp.4394-4400. 10.1109/TED.2023.3282194 . hal-04253408

**HAL Id: hal-04253408**

**<https://cnrs.hal.science/hal-04253408>**

Submitted on 16 Nov 2023

**HAL** is a multi-disciplinary open access archive for the deposit and dissemination of scientific research documents, whether they are published or not. The documents may come from teaching and research institutions in France or abroad, or from public or private research centers.

L'archive ouverte pluridisciplinaire **HAL**, est destinée au dépôt et à la diffusion de documents scientifiques de niveau recherche, publiés ou non, émanant des établissements d'enseignement et de recherche français ou étrangers, des laboratoires publics ou privés.

# Compact Efficient and Frequency Tunable Relativistic Magnetron With Reducing Coaxial Section and Tilted Tuners

Yannick Delvert<sup>1</sup>, Antoine Chauloux<sup>1</sup>, Jean-Christophe Diot<sup>1</sup>, Thierry Chanconie<sup>1</sup>,  
Nicolas Ribière-Tharaud<sup>1</sup>, and Philippe Lévêque<sup>1</sup>

**Abstract**—In this article, we present a compact efficient and frequency tunable relativistic magnetron (RM) with what we have named a reducing coaxial section (RCS) and with tilted tuners. The RCS is a conical-shaped part inserted in front of the output window. The design is adapted to the compact Marx generator of the Concept Léger Aéroporté d’illuminateur RadioElectrique (CEA)-Gramat demonstrator—Commissariat à l’Energie Atomique et aux Energies Alternatives (CLAIRE)—and meets technical requirements such as input impedance (specifically during frequency shifting), mechanical dimensions, power handling capacity, and electromagnetic (EM) mode. Special care has been taken to lower the EM mode competition, which occurs with specific geometry, extraction waveguide with high dimensions, and/or frequency shifting. To mitigate this effect, the output waveguide diameter was decreased by means of the RCS design. Another challenge was to operate frequency shifting by adding tuners while maintaining high power handling. The premise is that cathode endcap spheres and tilted tuners theoretically reduce the electric field strength from 600 to 280 kV/cm. Particle-in-cell (PIC) simulation exhibits an output power (averaged over the pulse duration) that reaches 680 MW at 1.85 GHz. The corresponding maximum power efficiency is about 50% when the applied voltage is 380 kV, and the current intensity is about 3.8 kA. The frequency operating range is above 19% from 1.85 to 2.25 GHz.

**Index Terms**—Frequency shifting, high power microwave (HPM), particle-in-cell (PIC) simulation, reducing coaxial section (RCS), relativistic magnetron (RM), tilted tuners.

## I. INTRODUCTION

TODAY, relativistic frequency tunable magnetrons seem to be the most mature high-power microwave (HPM) tubes capable of achieving high-power efficiency over a wide frequency range. Indeed, many researchers have contributed

Manuscript received 23 March 2023; revised 10 May 2023; accepted 29 May 2023. This work was supported by the Direction Générale de l’Armement (DGA). The review of this article was arranged by Editor E. Choi. (Corresponding author: Yannick Delvert.)

Yannick Delvert, Antoine Chauloux, Jean-Christophe Diot, and Thierry Chanconie are with the French Alternatives Energies and Atomic Energy Commission, CEA DAM Gramat, 46500 Gramat, France (e-mail: delvert.yannick@laposte.net).

Nicolas Ribière-Tharaud is with the French Alternatives Energies and Atomic Energy Commission, CEA DAM Ile de France, Bruyères-le-Châtel, 91297 Arpajon, France.

Philippe Lévêque is with the Xlim Research Institute, CNRS UMR 7252, 87060 Limoges, France.

Color versions of one or more figures in this article are available at <https://doi.org/10.1109/TED.2023.3282194>.

Digital Object Identifier 10.1109/TED.2023.3282194

to enhancing the performances over the last decade, either by increasing power efficiency, by improving compactness, or by reducing pulse-shortening effects [1], [2], [3], [4], [5], [6], [7], [8], [9], [10], [11], [12], [13], [14], [15], [16], [17], [18], [19], [20], [21].

Among significant progress in recent years, geometries based on an efficient structure with all-cavity electromagnetic (EM) radial extraction by coupling slots have been extensively described in other scientific papers [9], [10], [11], [12], [14]. A design introduced in 2012 [22], shows good performance with improved compactness. In addition, to avoid mode competition effects, the diameter of the coaxial wave extraction output can be reduced, with adjustments to cavity depth and the A–K gap as in the example [12]. However, this approach may not be suitable for low-frequency operation, or guarantee of a high-power handling capacity.

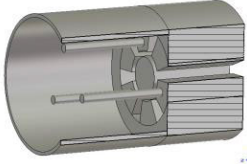
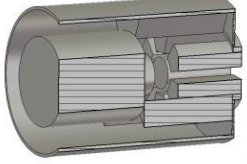
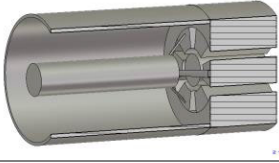
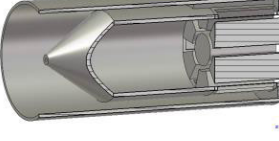
Inserting tuners into anode cavities [23], [24], [25] is a known and relatively efficient method of shifting the operating frequency. This approach has already been successfully tested and published [26]. The tuner technique is compatible with the efficient all-cavity EM radial extraction by using coupling slots and has been demonstrated in tests [25].

In this article, we study a magnetron prototype with a reducing coaxial section (RCS), which suppresses mode competition during propagation and theoretically ensures high-power handling capacity. The named RCS is a conical-shaped part inserted in front of the output window. Large sphere endcaps and tilted tuners were used to drastically reduce the electric field reinforcements and enable frequency shifting.

The proposed magnetron must propagate a transverse EM (TEM) or transverse magnetic (TM) output mode— $TM_{01}$ —over the bandwidth, to fit the topology of a structure such as the antenna used at Concept Léger Aéroporté d’illuminateur RadioElectrique (CEA)-Gramat [27]. The relativistic magnetron (RM) operating frequency is expected to be near 2 GHz. As the prototype must be connected to the compact HPM Marx generator of the CEA-Gramat demonstrator Commissariat à l’Energie Atomique et aux Energies Alternatives (CLAIRE) [28], the input impedance must be close to 100  $\Omega$ . The design has to be as compact as possible.

Section II of this article presents a method to select an efficient RM topology from research and some theoretical formulae. Section III gives the results of four studies, to design a RM prototype, theoretically achievable for experimental trials. Conclusions are given in Section IV.

**TABLE I**  
DESIGNS OF FOUR WAVE EXTRACTIONS FOR  
AN S-PARAMETERS EVALUATION

3D Designs	Extraction features
 (a)	<ul style="list-style-type: none"> <li>○ <b>Method:</b> conducting rods connected to the anode vanes of the A6 magnetron.</li> <li>○ <b>EM mode:</b> <math>TM_{01}</math></li> </ul>
 (b)	<ul style="list-style-type: none"> <li>○ <b>Method:</b> radial all-cavity extraction, into sectorial waveguide, into coaxial waveguide.</li> <li>○ <b>EM mode:</b> TEM</li> </ul>
 (c)	<ul style="list-style-type: none"> <li>○ <b>Method:</b> mode converter connected between 3 anode vanes and a coaxial central conductor.</li> <li>○ <b>EM mode:</b> TEM</li> </ul>
 (d)	<ul style="list-style-type: none"> <li>○ <b>Method:</b> radial all-cavity extraction by coupling slot, into coaxial waveguide, into mode converter.</li> <li>○ <b>EM mode:</b> <math>TM_{01}</math></li> </ul>

## II. SIMULATION MODEL

All the simulations were carried out using CST Microwave Studio software, which is very convenient for the study of vacuum electronic devices such as the magnetron.

### A. Time Solver Method for EM Output Evaluation

An S-parameter Time Solver from [16], enables transmission and reflection coefficient assessments. Four different wave extraction options were selected: (a) [16], (b) [12], (c) [29], and (d) [14]. This choice was dictated by performance, i.e., output EM mode, compactness, and output power efficiency. For the study, an A6 magnetron was chosen to compare only the extraction method, numerically reproduced as accurately as possible. S-parameters calculation required two waveguide ports. One is in contact with the anode block input or with the middle of A6 magnetron cavities, and the other one is connected to the output of the waveguide extraction.

From Table I and Fig. 1, four criteria guided the future RM design presented in this article. To reduce leakage currents and improve power efficiency, it is common to add endcaps at each end of the cathode [1], [2], [3], [4], [5], [6], [7], [8], [9], [10], [11], [12], [15], [16], [17]. Based on the 3-D designs, we judged the structure's ability to add endcaps while maintaining power-handling capacity. Structures (b) and (d) seem to leave more space than other types of extraction. Second, the broadband behavior criterion was identified in Fig. 1. The curves depend on the accuracy of designs reproduced from the scientific literature. According to Fig. 1, TEM extraction would appear to have a wider broadband behavior

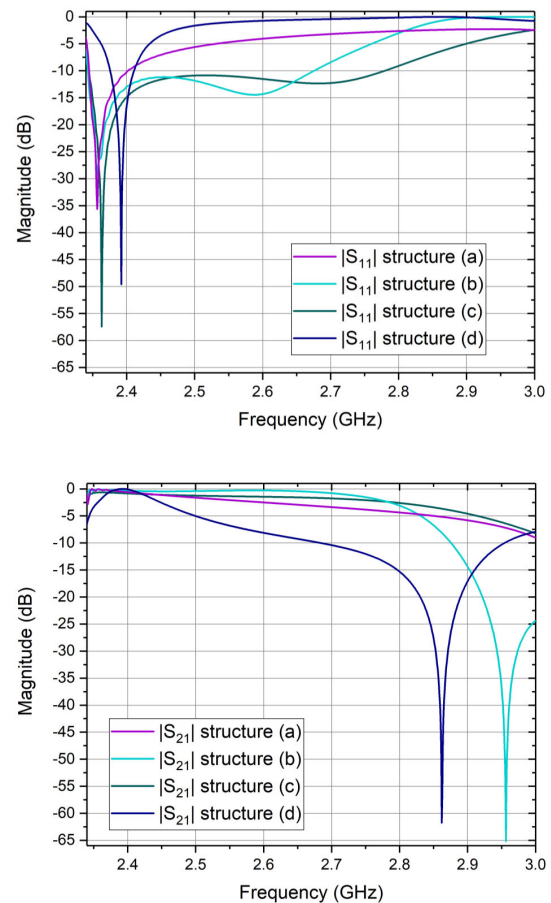


Fig. 1. S-parameters comparison between the four 3-D designs.

**TABLE II**  
CRITERIA FOR EM OUTPUT EVALUATION

Criterion \ Model	(a)	(b)	(c)	(d)
Endcaps integration		X		X
Broadband behavior		X	X	
Power efficiency	X	X	X	X
Compactness	X	X	X	

than  $TM_{01}$ . This point is crucial for frequency shifting. Finally, we identified the power efficiency and the compactness criteria described in the research papers. The efficiency criterion is set above 40% and the compactness is approximated by looking at the general volume in relation to the wavelength. The most compact are the structures (a) and (c), and (b) potentially, design.

All the criteria are summarized in Table II. For the reasons stated above, the radial all-cavity extraction structure toward the sectorial waveguide and the coaxial waveguide (inspired by Liu et al. [12]) was selected. To match the specifications, especially for Marx compatibility, the prototype was designed starting from the theoretical approach analyzed below.

## B. PIC Modeling—Theoretical Approach

A small number of cavities enables us to have a sufficient difference between frequency and azimuthal phase velocity [30], which avoids mode competition. Consequently, only six cavities were selected for the model.

The frequency approximation of the so-called efficient  $\pi$ -mode—where the phase difference between adjacent resonators is equal to  $\pi$ —is defined as follows [30]:

$$f_{\pi} \cong \frac{c}{4L_a} \quad (1)$$

where  $c$  is the speed of light and  $L_a$  is the resonator depth. In this work, cavity depth is set to 40 mm which leads to an expected frequency of about 1.88 GHz.

Resonator length can be approximatively defined also, by the following expression [30]:

$$h \cong 0.6\lambda \quad (2)$$

where  $\lambda$  is the wavelength. The calculated frequency gives a length of about 96 mm.

For the purpose of impedance matching reasons, the power source input impedance must be close to 100  $\Omega$ . Because the section between the HPM generator and the beginning of the RM cavities is a coaxial waveguide type, the input impedance can be approximated by [31]

$$Z_0 \cong 60 \left( \frac{\mu_r}{\varepsilon_r} \right)^{\frac{1}{2}} \ln \left( \frac{r_2}{r_1} \right) \quad (3)$$

where  $\mu_r$  is the relative permeability,  $\varepsilon_r$  is the relative permittivity, and  $r_1$  and  $r_2$  are the inner and outer radii of the coaxial cylindrical line. In this article,  $r_1$  and  $r_2$  are set to 10 and 55 mm, respectively, which leads to an input impedance of about 102  $\Omega$ .

The experimental applied voltage will be about 380 kV during 80 ns on about 100  $\Omega$  load. The necessary longitudinal magnetic field value can be framed by the Hull cutoff ( $B^*$ )—the limit to prevent breakdowns between anode and cathode—and the Buneman–Hartree condition ( $B_z$ )—the threshold to achieve resonance—from [30]

$$B^* = \frac{mc}{ed_e} \sqrt{\frac{2eV}{mc^2} + \left( \frac{eV}{mc^2} \right)^2} \quad (4)$$

$$B_z = \frac{mc^2 n}{e\omega_n r_a d_e} \left[ \frac{eV}{mc^2} + 1 - \sqrt{1 - \left( \frac{r_a \omega_n}{cn} \right)^2} \right] \quad (5)$$

where  $m$  and  $e$  are the mass and charge of an electron,  $c$  is the speed of light,  $d_e = (r_a^2 - r_c^2)/2 \times r_a$  is the effective gap in cylindrical geometry,  $r_a$  and  $r_c$  are the anode and cathode radii, respectively,  $V$  is the applied voltage, and  $\omega_n$  is the pulsation in radian per second of the  $n$ th azimuthal mode. In the formula,  $n$  is equal to  $N/2$ , where  $N$  is the number of cavities. Therefore, in the considered case of six cavities,  $n$  is equal to three. The pulsation  $\omega_n$  is defined as:  $\omega_n = 2\pi \times f_n$ , where  $f_n$  is the  $\pi$ -mode frequency. The longitudinal magnetic field value is framed between 0.14 and 0.17 T with the previous dimensions.

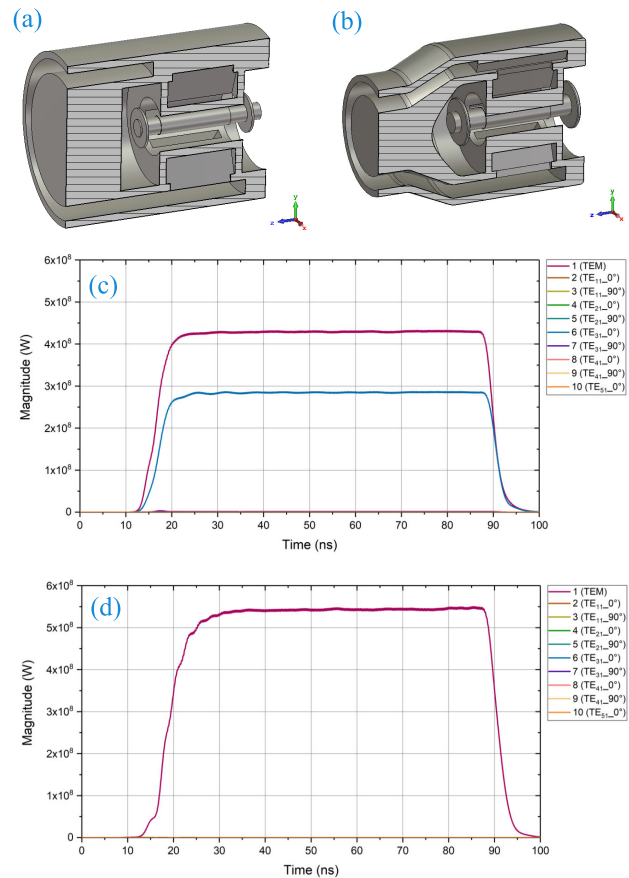


Fig. 2. (a) Comparison of the first ten CST EM output modes, between structures. (b) Same one with RCS. (c) First structure propagates a TEM and a TE<sub>31</sub> mode. (d) While the other propagates a quasi-pure TEM.

## III. NUMERICAL RESULTS

### A. Modes Competition in EM Extraction and the Means to Remove It

Thanks to the Time Solver method for EM output evaluation, and the previous theoretical formulae, a 3-D model was developed in Fig. 2(a), and enhanced under particle-in-cell (PIC) parametric simulations. For this, a pulsed voltage of 380 kV and 100 ns duration was applied between the anode and cathode, with five nanoseconds of rising and falling time. An explosive emission area was defined between the cathode endcaps. A waveguide port was added to the extraction window to view the first ten CST EM modes, clearly identified with nomenclature TE or TM modes, using information from other scientific papers. For each mode, a fast Fourier transform (FFT) determined the frequency, and a post-processing second-order Butterworth filter gave the average output power Fig. 2(c).

Because the RM presented in this article is composed of six cavities, a TE<sub>31</sub> non-desired EM mode is competing at the same frequency with the TEM mode which interests us. The TE<sub>31</sub> EM mode is time delayed compared to TEM, lowering the output power and the overall power efficiency. A way to improve it is to work on the mode competition. To remove the non-desired mode in the output propagation window, the coaxial waveguide cutoff frequencies were optimized.

Corresponding dimensions were computed as follows [32]:

$$TM_{mn} : \lambda_{c_{TM_{mn}}} = \frac{2\pi}{(c-1)\chi_{mn}}(a-b) \cong \frac{2}{n}(a-b) \\ n = 1, 2, 3, \dots \quad (6)$$

$$TE_{mn} : \lambda_{c_{TE_{m1}}} = \frac{2\pi}{(c+1)\chi'_{m1}}(a+b) \cong \frac{\pi}{m}(a+b) \\ m = 1, 2, 3, \dots \quad (7)$$

$$\lambda_{c_{TE_{mn}}} = \frac{2\pi}{(c-1)\chi'_{m1}}(a-b) \cong \frac{2}{n-1}(a-b) \\ n = 2, 3, 4, \dots \quad (8)$$

where  $a$  is the conductor radius,  $b$  is the central core radius,  $c$  is the factor ( $a/b$ ),  $\chi_{mn}$  is the  $m$ th root of the characteristic equation (9), and  $\chi'_{mn}$  is the  $m$ th root of the characteristic equation (10)

$$J_m(c\chi)N_m(\chi) - J_m(\chi)N_m(c\chi) = 0 \quad (9)$$

$$J_m'(c\chi')N_m'(\chi') - J_m'(\chi')N_m'(c\chi') = 0 \quad (10)$$

where  $J_m$  and  $N_m$  are the Bessel function of the first and second kind, and  $J_m'$  and  $N_m'$  are the derivative ones.  $\chi_{mn}$  and  $\chi'_{mn}$  first roots are listed in [32]. The  $TE_{31}$  non-desired mode was effectively cut in the propagation waveguide (but still not suppressed in the beam interaction region), by adding an RCS Fig. 2(b). The central core radius is reduced from 90 to 60 mm and the outer conductor radius from 106 to 76 mm. The non-desired EM mode is substantially decreased as the  $TE_{31}$  cutoff frequency switches from 1.43 to 2.05 GHz Fig. 2(d). It allows the power efficiency to rise from below 32.5% (only the efficiency of TEM mode but with competition) up to 44.5%.

Another method to propagate only a TEM mode without the RCS is to decrease the depth of the cavities and the A–K gap, so that the waveguide radii output is reduced [12], [16]. The first dimension was changed from 40 to 31 mm and the other from 29 to 18 mm. The thickness of the metal was also reduced for a final central core output radius of 60 mm compared to 90 mm previously. The TEM mode operation frequency (as  $TE_{31}$ ) was higher than in the initial topology (1.59 GHz before and 1.91 GHz after) but the  $TE_{31}$  cutoff frequency was nonetheless above (2.11 GHz) and without the RCS. A quasi-pure TEM output mode was generated with an average output power (on the pulse duration) of about 780 MW, at 1.91 GHz, a power efficiency of about 58%, and an input impedance of about 107  $\Omega$ .

The topology from this second method has the advantage of being easier to manufacture than the RCS. The frequency-agile operation (Section II-B) was studied from this structure.

### B. Frequency-Agile Operation by Tuners' Introduction

An efficient method to change the frequency operation is to modify the length of the cavities by inserting tuners. Several topologies were tested (cylinder insertion, a vertical plate, and horizontal blades). The most efficient way was to insert horizontal blades at the beginning of the anode block, as a means of progressively closing the opening cavities, instead of closing the coupling slots. PIC simulation led to a shift

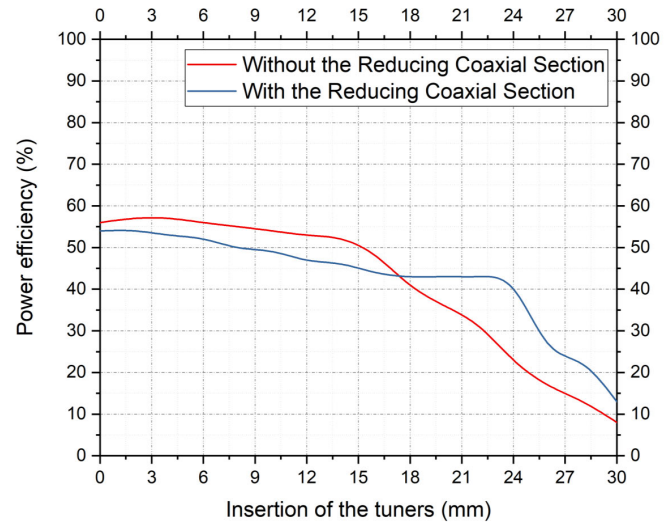


Fig. 3. Comparison of the power efficiency in relation to the insertion of the tuners between the solutions with and without the RCS.

in frequency from 1.89 to 2.24 GHz. When the tuners were inserted, the average output power decreased. The bandwidth between the maximum and the half output average power was then determined. Tuners ranging from 0 to 22 mm were introduced to ensure a frequency shift of about 17%. We observed that from the position of 16 to 22 mm, the power efficiency rapidly decreased by about 20% (see the curve without the RCS in Fig. 3). At this particular position, the operating frequency is about 2.11 GHz, i.e., the  $TE_{31}$  cutoff frequency. Consequently, mode competition reappeared and increased progressively after the insertion of the tuners. To prevent this phenomenon and because the dimensions were already reduced and could lead to breakdowns, the RCS was reapplied and appears to be the most relevant solution. To keep a sufficient margin, the extraction radii were set to 35 mm for the inner conductor and 51 mm for the outer conductor. Therefore, the  $TE_{31}$  cutoff frequency shifted from 2.11 to 3.33 GHz.

By reapplying an output diameter reduction, the power efficiency is maintained high over a broader frequency range. Indeed, mode competition was suppressed in the extraction waveguide, while the tuners are moving (see the curve with the RCS in Fig. 3). Note that the initial gap between the curves can be explained by the modification of the input impedance when the RCS is added, which is about 10  $\Omega$  lower. To compensate and be compatible with the Marx generator, diameter reduction was applied to the cathode.

The 3-D modeling with horizontal tuners and the RCS used for the study, is shown in Fig. 4. Two external magnetic field coils enable a quasi-flat B-field of about 0.21 T in the A–K gap. The average output power, the frequency shifting, the input impedance, and the power efficiency, in relation to the insertion of the tuners, are shown in Fig. 5. A quasi-pure TEM output mode was generated with a maximum average output power of up to 825 MW at the frequency of 1.87 GHz, with a power efficiency of about 58% and an input impedance compatible with the Marx generator. The RCS solution gave a frequency shift of about 21% from 1.87 to 2.31 GHz.

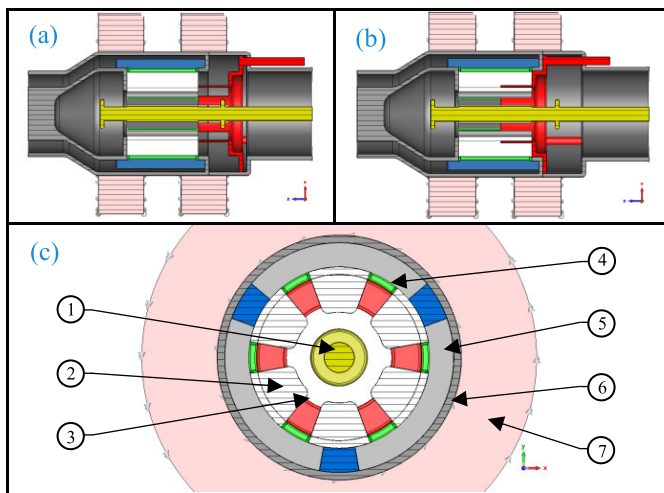


Fig. 4. (a) XZ cutting view, with tuners in initial position. (b) Fully introduced into cavities. (c) XY cutting view showing: 1—cathode; 2—anode vanes; 3—tuners; 4—coupling slots; 5—sectorial waveguide; 6—prototype body; and 7—magnetic coil.

### C. Power Handling Study and Structure Optimization

Relativistic sources are particularly challenging in terms of power handling because the applied voltage is over hundreds of kilovolts. The endcap regions are critical for RMs, especially when the structure is compact. A good method to highlight potential electrical breakdowns is to run an Electrostatic Solver simulation. The cathode was set to the potential of the Marx generator of interest (380 kV), and the tube body is set to null. A visualization of the study is represented in Fig. 6. The result Fig. 6(a) highlights that endcaps could lead to breakdown since the electrical field is over 600 kV/cm. To verify it, an evaluation of parasitic electron emission was run in PIC simulations. The entire cathode surface was defined as stainless steel electron emitter with a threshold in the range of 300–350 kV/cm [31]. The cathode center region was set with the explosive emission threshold of graphite reduced to 180 kV/cm [33]. The two thresholds were used as a theoretical approach to set a limit value and may not represent the experimental phenomena. The explosive electron emission depends on vacuum quality and surface finishes. Nevertheless, the PIC simulation confirms that the proposed endcaps lead to a massive electron emission and thus need further optimization.

Several solutions are proposed in this article. The first concerns the bend radius of the endcaps. The lower the bend radius, the higher the electrical field. Consequently, large sphere geometry was used instead of the small plates previously. Second, to increase the space between the input endcap and the frequency shifting pieces, original tilted tuners seem to be a solution. This would appear to be the best compromise between a frequency-shifting solution with the vertical tuners, which are effective for low input impedance variation, and the horizontal tuners introduced in Section II-B, which are an efficient solution. Third, to decrease the field strength in the final endcap region, a 40 mm coaxial waveguide

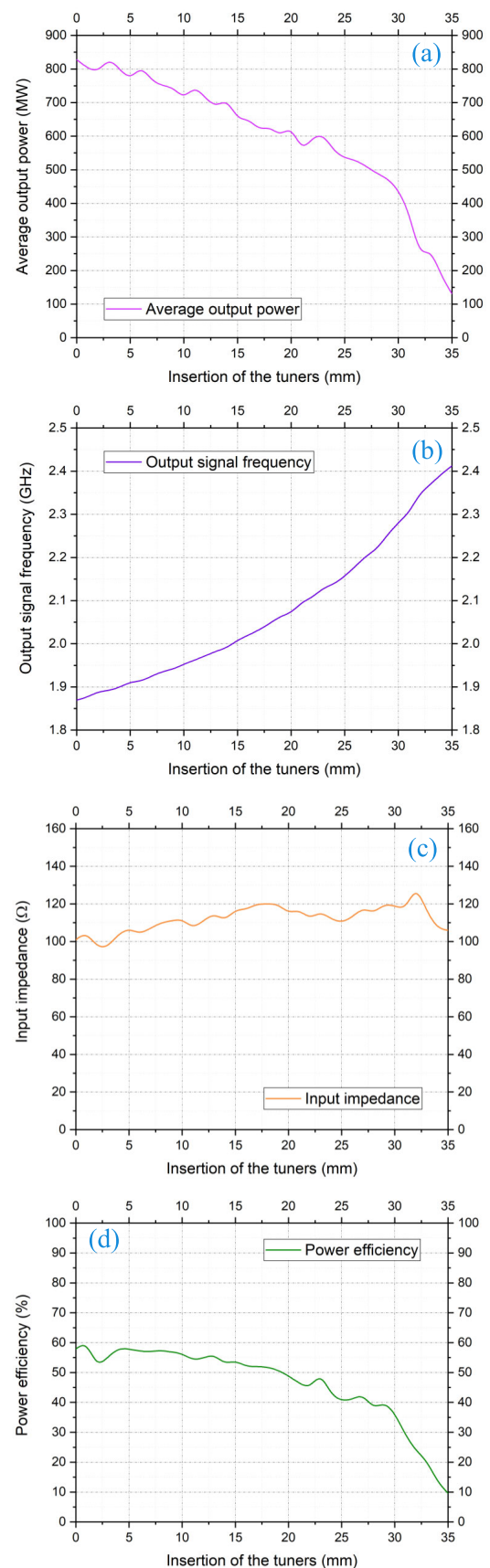


Fig. 5. (a) Summary of performances with representation of average output power, (b) frequency shifting, (c) input impedance, and (d) power efficiency, in relation to the insertion of the tuners.

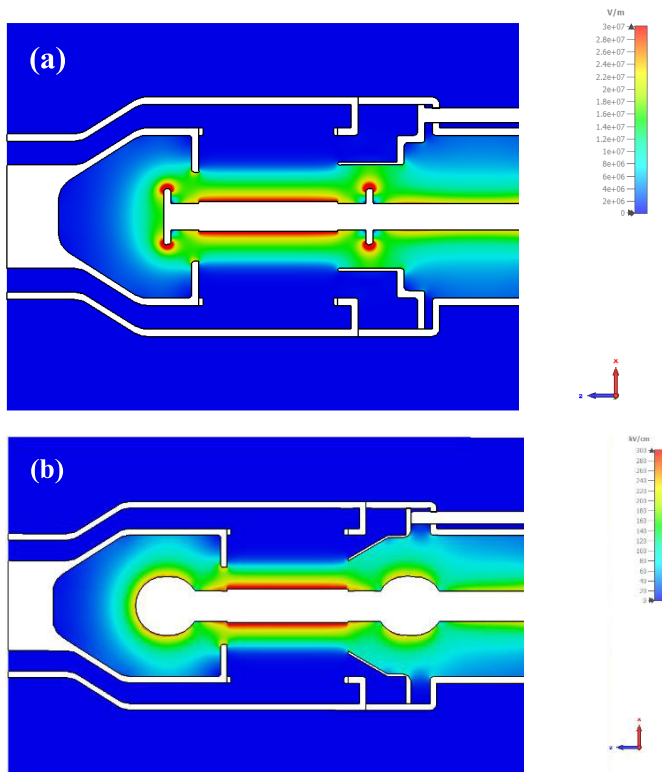


Fig. 6. (a) Electrostatic study results with an XZ cutting visualization, showing the initial case of the Section III-B. (b) Optimized structure with tilted tuners, now achievable for experimental trials.

was added before the diameter reduction, to leave more space between the endcap and the RCS. These modifications lead to a significant reduction of the static electrical field around the endcap from about 600 to about 280 kV/cm, which is below the theoretical stainless steel explosive emission threshold Fig. 6(b).

Because the topology is different from the structure in Section III-B, PIC simulations were run again, taking into account the previously mentioned theoretical emission parameters of graphite and stainless steel. The results obtained show that the power efficiency now reaches about 50% maximum compared with 58% before, and an average output power of about 680 MW. The frequency shifting is now about 19.5% from 1.85 to 2.25 GHz.

The new topology is slightly less efficient than the structure with plate endcaps and horizontal tuners. It could be explained by the quality factor of the resonant structure. Plate endcaps and horizontal tuners could be indeed more efficient to close the A–K gap in comparison with large spheres and tilted tuners. However, the power handling benefit is higher and our RM is now theoretically compatible with experimental trials.

#### D. From Modeling to Experimental Validation

PIC simulations are complex and time-consuming, especially when the number of emission points on the cathode surface is significant, and the number of mesh cells is high. It is important to notice that plasma expansion, thermal effects, and X-ray bremsstrahlung emissions, have not previously been considered. Indeed, these dynamic phenomena are strongly dependent on experimental conditions. For this reason,

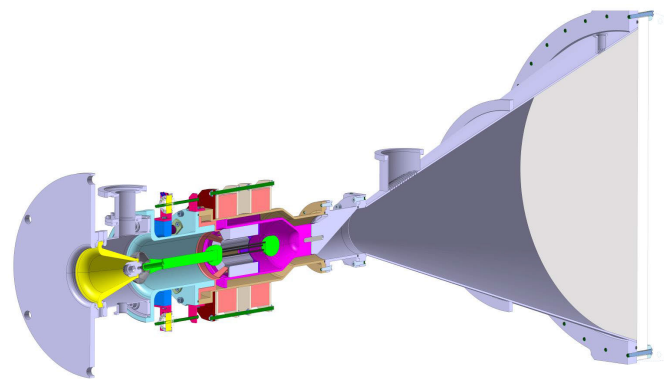


Fig. 7. Final numerical prototype model theoretically achievable for experimental trials, and compatible with CLAIRE HPM generator.

experimental validation is the only way to obtain the real performances of the proposed RM and HPM devices in general. To make it technically achievable, some additions were necessary. Four external motors and a vacuum accordion were added for the tuners to move. At the input, the waveguide and cathode were adapted to the Marx generator interface. The cathode was slipped into a trapezoidal mechanic piece to protect the generator from any electrons moving back toward it. Plates and threaded rods were also added to position the coils. All the magnetron mechanic pieces underwent electrolytic polishing, to ensure better surface finishes, especially for and around the cathode body.

Concerning the radiation of the TEM mode, before the use of a complex antenna such as the structure [27] used at CEA-Gramat in X-band, a simple solution was designed to validate the prototype. A conical horn antenna with a large aperture, closed by a PolyTetraFluoroEthylene (PTFE) disk, will be used in future tests, to radiate a powerful electrical field. On the band which concerns us, the gain achieved by this antenna is about 20 dB. To fit the RM output coaxial waveguide and the conical antenna, a mode converter from TEM to  $TE_{11}$  has also been designed, from [34] and [35]. This choice was made because of the need to experimentally position a receiving horn at several meters, in the axis of the antenna. A main pump coupled with two turbo pumping systems (one at the input of the HPM tube and another at the input of the conical antenna), will be added to ensure a strong vacuum, at a pressure below  $10^{-5}$  mbar. The complete prototype is shown in Fig. 7.

Pulse shortening is a problem for RM when using a solid cathode, because of plasma expansion toward the anode [7]. Lately, there has been a spike in interest in the development of new cathode topology for RMs, concerning transparent cathode [36], and most recently, the virtual cathode such as the split virtual cathode [7] to tackle cathode plasma-related issues. To anticipate and try to reduce the plasma problem, five cathodes will be manufactured. Experimental trials will be run with three solid cathodes of different diameters, and also with three and six-rod transparent cathodes.

## IV. CONCLUSION

We designed a compact efficient and frequency tunable RM with a TEM output mode. An RCS was enhanced to

maximize power efficiency over a larger frequency range. This option was preferred to an alternative based on dimension reduction, to mitigate the risk of breakdowns. In addition, for experimental feasibility reasons, large spheres and original tilted tuners discussed in this article were inserted to drastically reduce the static electrical field. As a result, 680 MW output power at the frequency of 1.82 GHz can be expected with a 50% power efficiency. The maximum frequency shifting range is above 19% from 1.85 to 2.25 GHz. The prototype can be connected to the Marx generator CLAIRE at CEA-Gramat. Consequently, the overall solution is relatively compact.

This RM prototype will be experimentally tested. Performances will be compared to simulation results in order to validate the modeling approach. Upon operation, a cathode plasma could form and expand. Such an effect could lead to pulse shortening. Therefore, a transparent cathode with three and six-rod will be manufactured to prevent this unwanted phenomenon.

## REFERENCES

- [1] C. He et al., "Preliminary experimental study on a compact relativistic magnetron with diffraction output of TEM mode," *IEEE Trans. Electron Devices*, vol. 70, no. 1, pp. 302–306, Jan. 2023.
- [2] R. Cheng et al., "Multiport relativistic magnetron for phased array application," *IEEE Trans. Electron Devices*, vol. 69, no. 3, pp. 1423–1428, Mar. 2022.
- [3] Y. E. Krasik et al., "An advanced relativistic magnetron operating with a split cathode and separated anode segments," *J. Appl. Phys.*, vol. 131, no. 2, Jan. 2022, Art. no. 023301, doi: [10.1063/5.0080421](https://doi.org/10.1063/5.0080421).
- [4] Z. Liu, Y. Fan, H. Xu, A. Li, X. Wang, and D. Shi, "A high efficiency and high power L-band relativistic magnetron with all-cavity extraction," *Rev. Sci. Instrum.*, vol. 93, no. 10, Oct. 2022, Art. no. 104710, doi: [10.1063/5.0095784](https://doi.org/10.1063/5.0095784).
- [5] Z. Liu, Y. Fan, X. Wang, S. Li, and A. Li, "An improved high-efficiency relativistic magnetron with a novel cathode endcap," *AIP Adv.*, vol. 11, no. 2, Feb. 2021, Art. no. 025239, doi: [10.1063/5.0028617](https://doi.org/10.1063/5.0028617).
- [6] X. Fang et al., "S-band GW-level relativistic magnetron operating at relatively low applied voltage," *IEEE Trans. Microw. Theory Techn.*, vol. 70, no. 2, pp. 1111–1118, Feb. 2022.
- [7] J. G. Leopold et al., "Experimental and numerical study of a split cathode fed relativistic magnetron," *J. Appl. Phys.*, vol. 130, no. 3, Jul. 2021, Art. no. 034501, doi: [10.1063/5.0055118](https://doi.org/10.1063/5.0055118).
- [8] X. Fang, F. Qin, L. Lei, S. Xu, Y. Zhang, and D. Wang, "Compact high efficiency relativistic magnetron with TE<sub>11</sub> mode output," *IEEE Trans. Electron Devices*, vol. 68, no. 8, pp. 4110–4115, Aug. 2021.
- [9] R. Cheng et al., "Efficient relativistic magnetron with a split cathode," *IEEE Trans. Electron Devices*, vol. 68, no. 5, pp. 2480–2484, May 2021.
- [10] J. G. Leopold, E. Krasik, Y. Hadas, and E. Schamiloglu, "An axial output relativistic magnetron fed by a split cathode and magnetically insulated by a low-power solenoid," *IEEE Trans. Electron Devices*, vol. 68, no. 10, pp. 5227–5231, Oct. 2021, doi: [10.1109/TED.2021.3105942](https://doi.org/10.1109/TED.2021.3105942).
- [11] C. He et al., "Compact dual-frequency relativistic magnetron with TEM mode output," *IEEE Trans. Electron Devices*, vol. 67, no. 10, pp. 4421–4425, Oct. 2020.
- [12] Z. Liu, Y. Fan, X. Wang, D. Shi, A. Li, and Y. Yu, "A high-efficiency relativistic magnetron with a novel all-cavity extraction structure," *AIP Adv.*, vol. 10, no. 3, Mar. 2020, Art. no. 035104, doi: [10.1063/1.5102151](https://doi.org/10.1063/1.5102151).
- [13] M. Sattarov et al., "Highly efficient compact gigawatt-level microwave source using relativistic electrons: Radial relativistic magnetron," *Electron. Lett.*, vol. 56, no. 11, pp. 556–559, May 2020.
- [14] R. Cheng et al., "An efficient all cavity axial extraction relativistic magnetron with virtual cathode," *IEEE Trans. Electron Devices*, vol. 67, no. 5, pp. 2165–2169, May 2020, doi: [10.1109/TED.2020.2978888](https://doi.org/10.1109/TED.2020.2978888).
- [15] C. He, T. Li, B. Hu, H. Wang, K. Wang, and J. Li, "The characteristics research on A6 relativistic magnetron with diffraction output operating in the negative first harmonic of 2 $\pi$ /3 mode," *IEEE Trans. Plasma Sci.*, vol. 47, no. 8, pp. 3967–3973, Aug. 2019.
- [16] F. Qin, S. Xu, L. Lei, B. Ju, and D. Wang, "A compact relativistic magnetron with lower output mode," *IEEE Trans. Electron Devices*, vol. 66, no. 4, pp. 1960–1964, Apr. 2019.
- [17] C. Leach, S. Prasad, M. I. Fuks, J. Buchenauer, J. W. McConaha, and E. Schamiloglu, "Experimental demonstration of a high-efficiency relativistic magnetron with diffraction output with spherical cathode endcap," *IEEE Trans. Plasma Sci.*, vol. 45, no. 2, pp. 282–288, Feb. 2017.
- [18] D.-F. Shi, B.-L. Qian, H.-G. Wang, W. Li, and G.-X. Du, "A frequency tunable relativistic magnetron with a wide operation regime," *AIP Adv.*, vol. 7, no. 2, Feb. 2017, Art. no. 025010, doi: [10.1063/1.4971760](https://doi.org/10.1063/1.4971760).
- [19] X.-Y. Wang, Y.-W. Fan, D.-F. Shi, and T. Shu, "A high-efficiency relativistic magnetron with the filled dielectric," *Phys. Plasmas*, vol. 23, no. 7, Jul. 2016, Art. no. 073103, doi: [10.1063/1.4956460](https://doi.org/10.1063/1.4956460).
- [20] D. Shi, B. Qian, H. Wang, W. Li, and Y. Wang, "A compact mode conversion configuration in relativistic magnetron with a TE<sub>10</sub> output mode," *IEEE Trans. Plasma Sci.*, vol. 43, no. 10, pp. 3512–3516, Oct. 2015.
- [21] M. Liu, C. Liu, M. I. Fuks, and E. Schamiloglu, "Operation characteristics of 12-cavity relativistic magnetron with single-stepped cavities," *IEEE Trans. Plasma Sci.*, vol. 42, no. 10, pp. 3283–3287, Oct. 2014.
- [22] B. W. Hoff, A. D. Greenwood, P. J. Mardahl, and M. D. Haworth, "All cavity-magnetron axial extraction technique," *IEEE Trans. Plasma Sci.*, vol. 40, no. 11, pp. 3046–3051, Nov. 2012, doi: [10.1109/TPS.2012.2217758](https://doi.org/10.1109/TPS.2012.2217758).
- [23] H. Kim and J. Choi, "Three-dimensional particle-in-cell simulation study of a frequency tunable relativistic magnetron," *IEEE Trans. Dielectr. Electr. Insul.*, vol. 14, no. 4, pp. 1045–1049, Aug. 2007, doi: [10.1109/TDEI.2007.4286546](https://doi.org/10.1109/TDEI.2007.4286546).
- [24] F. Qin, Y. Zhang, S. Xu, L. Lei, B. Ju, and D. Wang, "A frequency-agile relativistic magnetron with axial tuning," *IEEE Electron Device Lett.*, vol. 41, no. 5, pp. 781–783, May 2020, doi: [10.1109/LED.2020.2984096](https://doi.org/10.1109/LED.2020.2984096).
- [25] F. Qin et al., "A cross-band tunable relativistic magnetron with all cavity axial extraction," *IEEE Trans. Electron Devices*, vol. 70, no. 3, pp. 1283–1287, Mar. 2023, doi: [10.1109/TED.2023.3238387](https://doi.org/10.1109/TED.2023.3238387).
- [26] S. J. Levine, D. B. Harteneck, and H. D. Price, "Frequency agile relativistic magnetrons," *Proc. SPIE*, vol. 2557, pp. 74–79, Sep. 1995, doi: [10.1117/12.218536](https://doi.org/10.1117/12.218536).
- [27] S. B. Pottier, F. Hamm, D. Jousse, P. Sirot, F. T. Talom, and R. Vézinet, "High pulsed power compact antenna for high-power microwaves applications," *IEEE Trans. Plasma Sci.*, vol. 42, no. 6, pp. 1515–1521, Jun. 2014, doi: [10.1109/TPS.2014.2321416](https://doi.org/10.1109/TPS.2014.2321416).
- [28] R. Vézinet et al., "Development of a compact narrow-band high power microwave system," in *Proc. IEEE Int. Power Modulator High Voltage Conf. (IPMHVC)*, Jul. 2016, pp. 132–135, doi: [10.1109/IPMHVC.2016.8012912](https://doi.org/10.1109/IPMHVC.2016.8012912).
- [29] C. He et al., "Compact L-band relativistic magnetron with diffraction output of TEM mode," *IEEE Trans. Electron Devices*, vol. 66, no. 12, pp. 5327–5332, Dec. 2019, doi: [10.1109/TED.2019.2945836](https://doi.org/10.1109/TED.2019.2945836).
- [30] J. Benford, J. A. Swegle, and E. Schamiloglu, *High Power Microwaves*, 3rd ed. Boca Raton, FL, USA: CRC Press, 2016, pp. 231–272.
- [31] S. T. Pai and Q. Zhang, "Introduction to high power pulse technology," *Adv. Ser. Electr. Comput. Eng.*, vol. 10, p. 104, Jan. 1995.
- [32] N. Marcuvitz, *Waveguide Handbook*. New York, NY, USA: McGraw-Hill, 1951, pp. 72–80.
- [33] R. Chandra et al., "Explosive emission properties of cathode materials in relativistic electron beam generation," *IEEE Trans. Plasma Sci.*, vol. 42, no. 11, pp. 3491–3497, Nov. 2014, doi: [10.1109/TPS.2014.2356615](https://doi.org/10.1109/TPS.2014.2356615).
- [34] S. J. Hosseini, "A circularly polarized TEM to TE<sub>11</sub> mode converter antenna," *J. Eng.*, vol. 2022, no. 2, pp. 216–222, Feb. 2022, doi: [10.1049/tje2.12110](https://doi.org/10.1049/tje2.12110).
- [35] D. N. Bykov, N. M. Bykov, and I. K. Kurkan, "Wideband TEM-TE<sub>11</sub> mode converter for HPM applications," *J. Phys., Conf.*, vol. 830, May 2017, Art. no. 012037, doi: [10.1088/1742-6596/830/1/012037](https://doi.org/10.1088/1742-6596/830/1/012037).
- [36] M. Fuks and E. Schamiloglu, "Rapid start of oscillations in a magnetron with a 'transparent' cathode," *Phys. Rev. Lett.*, vol. 95, no. 20, 2005, Art. no. 205101, doi: [10.1103/PhysRevLett.95.205101](https://doi.org/10.1103/PhysRevLett.95.205101).